The paper was published in the proceedings of the 11th International Conference on Physical Modelling in Geotechnics (ICPMG2026) and was edited by Ioannis Anastasopoulos. The conference was held from June 8th to June 12th 2026 in Zurich, Switzerland.

The influence of soil preparation methods on liquefaction behavior in centrifuge modeling

N. Takamatsu
Kyoto University, Kyoto, Japan, takamatsu.nao.76v@st.kyoto-u.ac.jp

J. Florez, K. Ueda, R. Uzuoka
Kyoto University, Kyoto, Japan,
florez.jhon.28s@st.kyoto-u.ac.jp, ueda.kyohei.2v@kyoto-u.ac.jp, uzuoka.ryosuke.6z@kyoto-u.ac.jp

ABSTRACT: Soil particle structure is a key factor influencing liquefaction behavior. This study investigates the effects of different sample preparation methods, including water pluviation and dry tamping (with four-layer or eight-layer compaction), on liquefaction in centrifuge models prepared at the same relative density. Two shaking events were conducted to evaluate changes in ground response, which were measured by miniature cone penetration tests conducted before and after each event.

1 INTRODUCTION

Soil particle structure is one of the key factors influencing liquefaction behaviour. Many previous studies have demonstrated that liquefaction resistance varies depending on sample preparation methods, and these findings are often based on results from cyclic undrained triaxial tests. In contrast, there are few studies about soil preparation methods in a geotechnical centrifuge.

In this study, centrifuge tests were conducted on soil models prepared using two different methods, including water pluviation and dry tamping under the same relative density conditions. Liquefaction behaviour was evaluated based on measurements of acceleration and pore water pressure. To further examine the degree of changes in soil fabric after shaking, two successive shaking events were applied. In addition, to assess changes in ground strength, cone penetration tests (CPTs) were performed before shaking as well as after each of the two shaking events.

2 CENTRIFUGE TESTING

2.1 Centrifuge facility

All tests were conducted at the Disaster Prevention Research Institute, Kyoto University. Table 1 shows the technical specifications of the centrifuge machine.

2.2 Scaling law

The experiment was conducted under a centrifugal acceleration of 40G. The scaling factors employed are detailed in Table 2 to facilitate the conversion from model scale to prototype scale.

Table 1 Technical Specifications of the Centrifuge Machine

Parameter	Value
Effective radius	2.5 m
Max payload	24 g-ton
Maximum centrifugal acceleration	200 g
Maximum number of rotations	260 rpm
Maximum payload at 50G	Dynamic:142.5 kg

Table 2 Scaling factors (Kutter, 1994)

Parameter	Ratio of model to prototype (a)
Length	$1/n$
Area	$1/n^2$
Volume	$1/n^3$
Stress	1
Strain	1
Force	$1/n^2$
Velocity	1
Acceleration	n
Frequency	n
Time (dynamic)	$1/n$

(a) n = centrifuge acceleration

2.3 Soil model

The centrifuge tests were conducted using the model shown in Fig. 1. The target relative density of the sand was set to 67.5%, and the model ground was prepared using Toyoura sand, a well-documented Japanese standard sand. Physical properties of Toyoura sand are shown in Table 3. Accelerometers and pore water pressure transducers were installed in pairs at every four layers within the model ground. Regarding the placement of the accelerometer, the transverse wall (perpendicular to the shaking) is highly susceptible to boundary condition effects, such as wave reflection. Therefore, a sufficient clearance of 12 cm (4.8 m in prototype scale) was maintained from this wall. In contrast, the influence of the longitudinal wall (parallel to the shaking) on the localized acceleration response was considered relatively minor and negligible. Consequently, due to the size constraints of the soil container, the accelerometer was installed at a distance of 3 cm (1.2 m in prototype scale) from the longitudinal wall. Similarly, the pore water pressure transducers were installed at a distance of 5 cm (2.0 m in prototype scale) from the longitudinal wall. This distance is considered sufficient to eliminate the influence of boundary friction on the measurements. CPTs were performed using a 6-mm-diameter miniature cone, and penetration was conducted before and after each shaking event at the locations indicated in Fig. 1(b), proceeding from left to right.

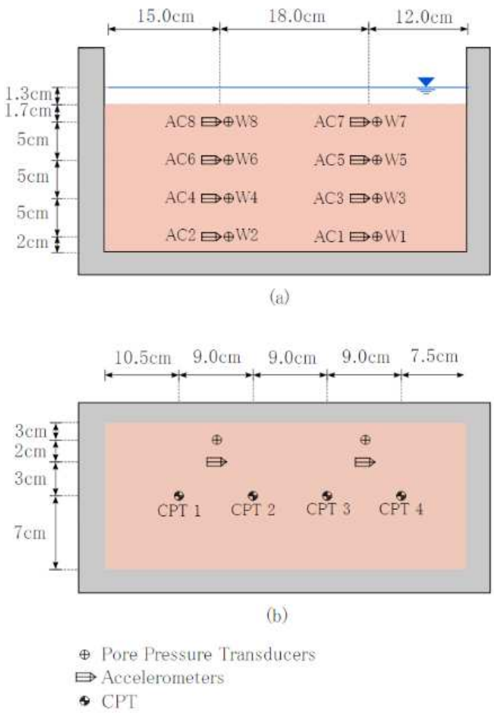

Figure 1. (a) Model ground layout, instrumentation (b) CPT locations

Table3 Physical properties of Toyoura sand

$d_{50}(mm)$	$G_s(g/cm^3)$	e_{max}	e_{min}
0.171	2.635	0.991	0.624

2.4 Soil preparation

a) Water pluviation (WP)
The sample was prepared by pluviating sand into a soil box filled with a 10-cm-deep viscous fluid solution. Pore pressure transducers and accelerometers were positioned at their planned locations using fishing lines and thin steel plates. The relative density was controlled using a vibrating device equipped with nine steel rods, each approximately 1 mm in diameter and spaced at 5-cm intervals.

b) Dry tamping with four-layer compaction (DT4)
The sample was constructed in four layers using a dry compaction method. Due to the arrangement of the measuring instruments, the thickness of the initial layer was adjusted. First, a 3.5 cm-thick layer of sand was placed and compacted, after which the upper 1.5 cm was loosened. Next, a 5 cm-thick layer of sand was added and compacted, and again the upper 1.5 cm was loosened. This procedure was repeated a total of four times to prepare the sample.

c) Dry tamping with eight-layer compaction (DT8)
The sample was constructed in eight layers using a dry compaction method. First, a 5-cm-thick layer of sand was placed and compacted. Next, 3 cm of sand was removed using a vacuum cleaner. Then, another 5-cm layer of sand was added and compacted, after which 2.5 cm of sand was removed by vacuum. This procedure was repeated a total of eight times.

2.5 Archived cases

A comprehensive summary of the detailed testing conditions is given in Table 4. The achieved waves in the three cases are shown in Fig. 2, which were measured by the accelerometer placed in the soil box.

Table 4. Comprehensive summary of the detailed testing conditions for the input wave, Dr and Sr.

Case	Input wave	Dr(%)	Sr(%)
WP	sine wave	67.5	95.583
DT4	Max:200Gal		99.60
DT8	50 loading cycles		99.90

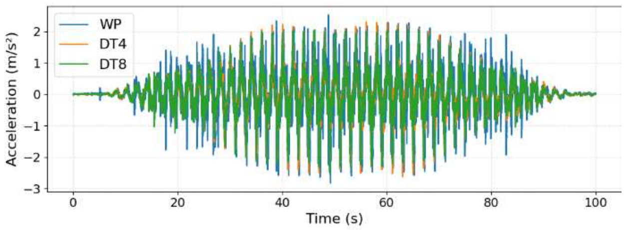

Figure 2. Achieved Acceleration responses in 3 cases

2.6 Testing procedures

Two shaking events were conducted, with CPTs performed before and after each shaking. Due to limitations of the centrifuge used in this study, it was impossible to perform shaking while the miniature cone was installed in the soil box. Therefore, the experimental sequence was arranged as presented in Table 5. This testing procedure was repeated twice and concluded with a CPT.

Table 5. Testing Procedure

	Procedures		
1	Install Miniature Cone		
2	Spinup	**6**	Spinup
3	CPT	**7**	Shaking
4	Spindown	**8**	Spindown
5	Remove Miniature Cone	**→1**	

3 TEST RESULT

3.1 CPT data correction process

The CPT data was corrected following the methodology described by Florez (2026). At shallow depths, soil resistance is insufficient to support the self-weight of the rod–cone assembly, causing the cone to penetrate prematurely. This results in a "data gap" where the sensor cannot record the load. To address this, the CPT data was corrected using the following procedure. The physical process observed during the initial penetration is illustrated schematically in Figure 3 and can be divided into three distinct stages:

Stage (a): Zero-penetration reference. The cone tip is initially positioned at the ground surface and restrained by an aluminium sheet to prevent downward movement under its own weight. This defines the true zero-penetration reference point.

Stage (b): Self-weight-driven penetration (Data gap). Once penetration begins, the aluminium sheet ruptures, and the rod–cone assembly accelerates downward under its own weight. It penetrates faster than the sleeve–load-cell system, causing a temporary separation. During this phase, displacement is recorded, but no valid tip resistance (load data) is captured. This stage ends when soil resistance balances the stress induced by self-weight, allowing the load cell to "catch up" and re-establish contact.

Stage (c): Load-cell engagement (Resumption of measurement). Continuous tip resistance measurements begin once contact is restored. Since the penetration depth at this stage already includes the displacement accumulated during the self-weight phase, the values must be corrected using Equation (1):

$$q_c^{corr} = q_c^{meas} + q_{rod-tip} \quad (1)$$

Subsequently, the penetration response during the Stage (b) data gap (from the origin (0,0) to the point of re-engagement) was reconstructed. While Florez (2026) suggested a logarithmic model for this phase, a linear interpolation was adopted in this study to simplify the initial resistance trend while maintaining consistency with the re-engagement point. This approach allows for a continuous and reliable penetration curve from the ground surface (0,0) to the final depth.

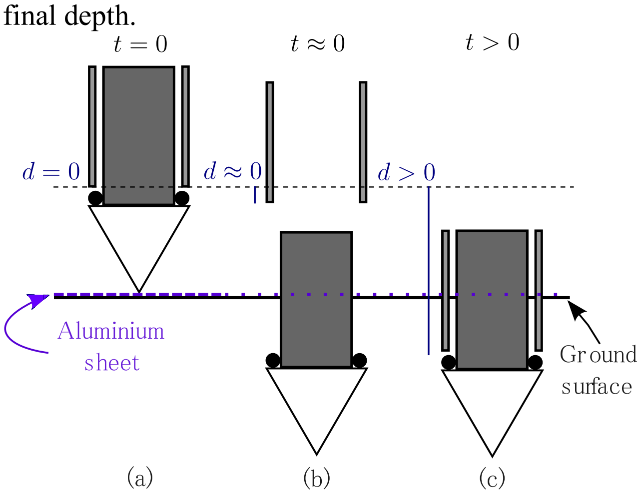

Figure 3. Stages of penetration at achieved gravity (50g) (a) Zero-penetration reference (b) Self-weight-driven penetration (c) Load-cell engagement. (Florez, 2026).

3.2 CPT results

The CPT results are shown in Fig. 4. The DT4 case exhibits a wavelike pattern, particularly before shaking. This indicates that the CPT clearly captures the compaction layers and that variability in soil strength exists among these layers, implying non-uniformity in the depth direction of the soil model. In contrast, for DT8, increasing the number of compaction layers results in an overall higher cone tip resistance throughout the soil profile and a more uniform soil structure along the depth.

In both dry tamping cases, only minor changes in cone tip resistance due to shaking are observed. However, in the WP case, the soil deposit is the most uniform among all preparation methods and shaking leads to an increase in cone tip resistance, particularly in deeper zones. Soil models prepared by the dry tamping method are generally considered to have an isotropic structure. Owing to this isotropy, it can be inferred that structural rearrangement due to shaking was less likely to occur.

3.3 Excess pore water pressure ratio and acceleration

Figs. 5, 7, and 9 present the excess pore water pressure ratio (r_u) and acceleration (ACC) responses for the WP, DT4, and DT8 cases. To clearly illustrate the pore pressure rise-up process and acceleration response, the plotting scale from 100 s to 500 s is compressed to 1/4 of the original plotting scale. This specific interval covers the period from the end of shaking until the excess pore water pressure (EPWP) dissipates to zero. The r_u $value$ is calculated by dividing the EPWP generated at a specific depth during shaking by the vertical effective stress at that same depth. Generally, liquefaction is considered to have occurred when the r_u value reaches or approaches 1. In this experiment, significant shaking caused the pore water pressure transducers, particularly those installed near the ground surface, to settle considerably into deeper positions. This settlement resulted in a substantial change in the vertical effective stress at the actual sensor locations when comparing the states before and after shaking. If r_u were calculated based solely on the initial pre-shaking vertical effective stress, the increased water pressure at the deeper post-settlement position would be divided by an underestimated stress value. This would lead to an erroneously high r_u value approaching 2. To address this discrepancy, the r_u values in this analysis were determined by dividing the measured pore water pressure by the average vertical effective stress derived from the sensor positions recorded both before and after the shaking.

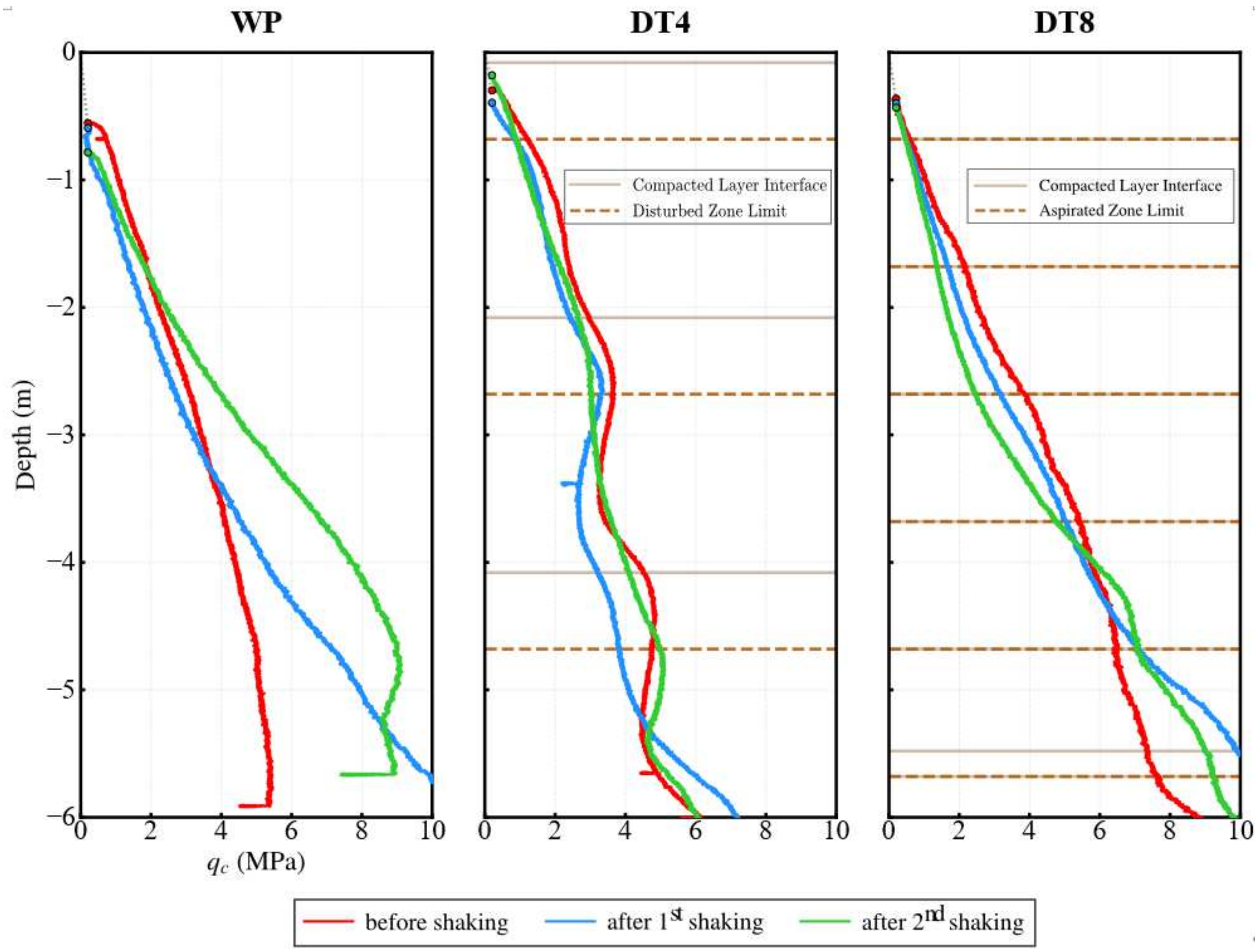

Figure 4. CPT results in WP, DT4 and DT8 (before shaking, after first shaking, after second shaking

Figures 6, 8, and 10 present the liquefaction timelines for the WP, DT4 and DT8 cases, respectively. Each bar represents the specific duration for which the r_u value exceeded the threshold of 1.0. Specifically, these timelines illustrate the period from the point when r_u value first reached 1.0 until it subsequently fell back below this threshold. The dashed vertical line indicates the end of the shaking

3.3.1 Water pluviation case

Fig. 5 presents the r_u and ACC results for the WP case, while Fig. 6 illustrates the corresponding liquefaction timelines. In both the first and second shaking events, liquefaction occurred at the installation depths of W3 and W5. Regarding the acceleration response, a significant de-amplification was observed at ACC3 and ACC5 toward the end of the shaking. This phenomenon can be attributed to the triggering of liquefaction, which led to a marked decrease in effective stress and shear stiffness, indicating substantial soil softening. Particularly in the behavior of W5 during the first shaking, the measured pore water pressure was higher after the shaking than before it. This suggests that significant settlement of the sensor occurred during the shaking event. Consequently, the calculated excess pore water pressure ratio $r_u = 1$ appears to have increased substantially following the completion of the shaking, , leading to the liquefaction timeline indicating that liquefaction occurred and persisted even after the shaking ended. Furthermore, the maximum r_u value in the second shaking event was relatively lower compared to the first shaking, with this tendency being more significant in the deeper sensors. Accordingly, the duration of liquefaction in the second event was also reduced to approximately half of that observed in the first event.

3.3.2 Dry tamping (four-layer) case

Fig. 7 presents the r_u and ACC results for the DT4 case, while Fig. 8 illustrates the corresponding liquefaction timelines. Similar to the WP case, liquefaction occurred at W3 and W5 during both shaking events. Regarding the acceleration response, a significant de-amplification was observed at ACC5 as r_u approached 1 in both shaking events, and dilation spikes were also recorded, particularly during the first shaking. Similar to the WP again, in the case of W5 during the first shaking, the measured pore water pressure was higher after the shaking than before it. This suggests that significant settlement of the sensor occurred during the shaking event. In contrast to the WP case, the maximum r_u values during the second shaking did not show a significant difference compared to those observed in the first shaking. Accordingly, the duration of liquefaction in the second event remained nearly the same as that observed in the first event.

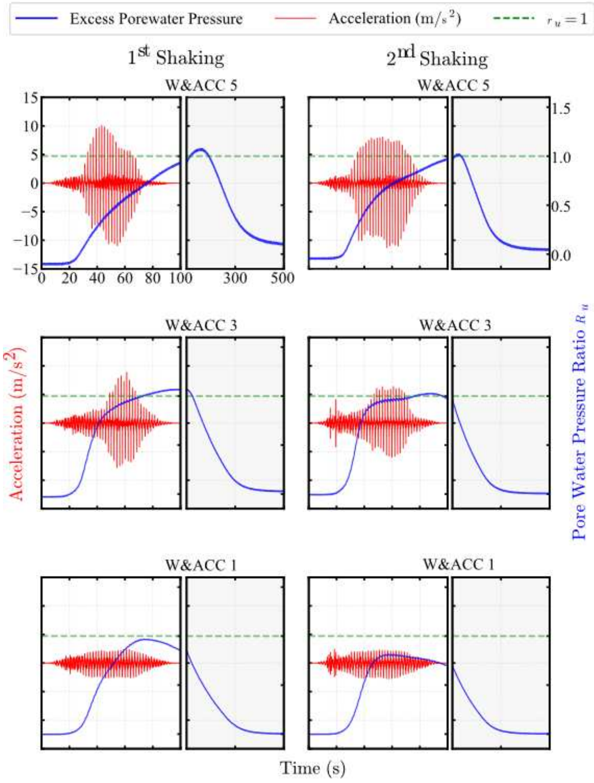

Figure 5. EPWP and ACC in WP case

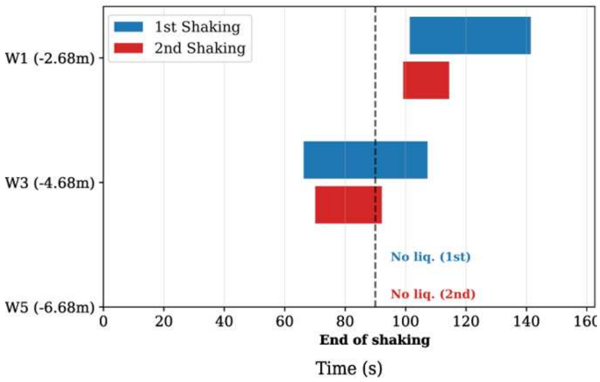

Figure 6. Liquefaction timeline for WP case. Horizontal bars indicate the onset and duration of liquefaction

3.3.3 Dry tamping (eight-layer) case

Fig. 9 presents the r_u and ACC results for the DT8 case, while Fig. 10 illustrates the corresponding liquefaction timelines. During both the first and second shaking events, liquefaction occurred at sensor W5, while a state close to liquefaction was observed at W3. In the acceleration records, dilation spikes were observed at ACC3 and ACC5 during the first shaking event. Similar to the other cases, the measured pore water pressure at W5 during the first shaking was higher after the shaking than before it, suggesting that significant settlement of the sensor occurred during the shaking. Furthermore, similar to the DT4 case, the maximum r_u values did not show a significant difference between the first and second shaking events. Consequently, the duration of liquefaction in the second event did not exhibit a marked reduction, unlike the significant shortening observed in the WP case.

3.3.4 Comparison of the three cases

Fig. 11 shows a comparison of EPWP ratio responses of the three cases during the first and second shaking events. In the DT4 case, the r_u increased more rapidly than in the other two cases. This can be attributed to the non-uniformity of the soil deposit between layers, where locally looser zones existed, as confirmed by the CPT results. This non-uniformity led to a faster build-up of excess pore water pressure compared with the DT8 case. In contrast, during the first shaking event, the WP case exhibited a more rapid increase in EPWP and reached higher r_u values compared to the DT8 case. However, during the second shaking, the r_u value in the WP case was lower than its first-shaking counterpart, resulting in responses that were almost comparable between the two cases in second shaking.

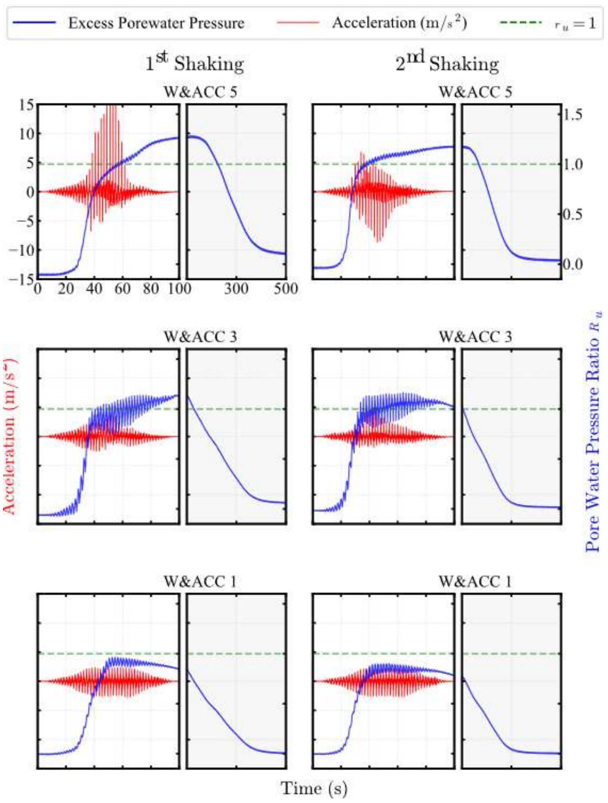

Figure 7. EPWP and ACC in DT4 case

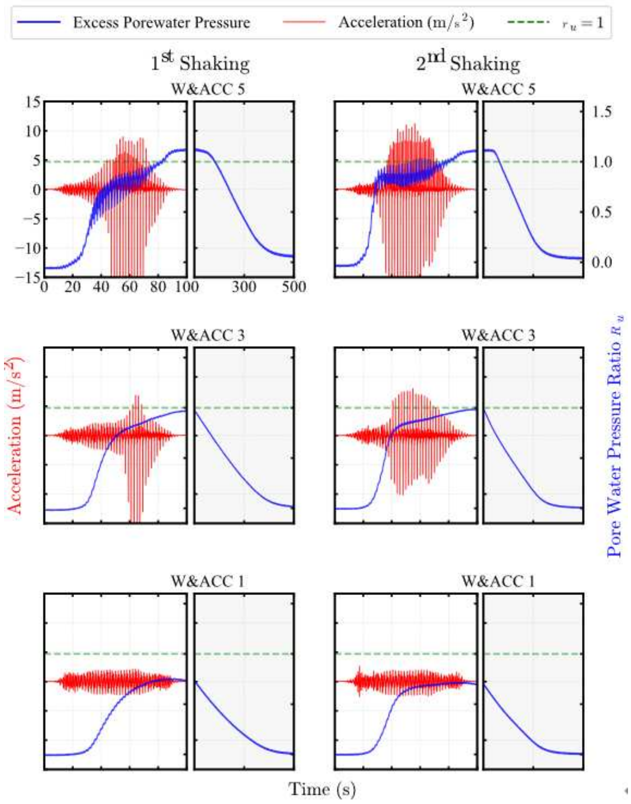

Figure 9. EPWP and ACC in DT8 case

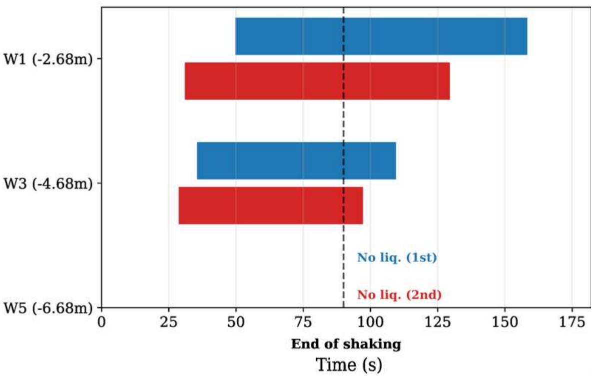

Figure 8. Liquefaction timeline for DT4 case. Horizontal bars indicate the onset and duration of liquefaction

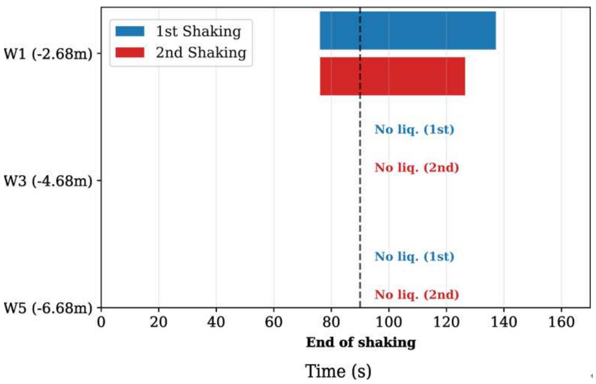

Figure 10. Liquefaction timeline for DT8 case. Horizontal bars indicate the onset and duration of liquefaction

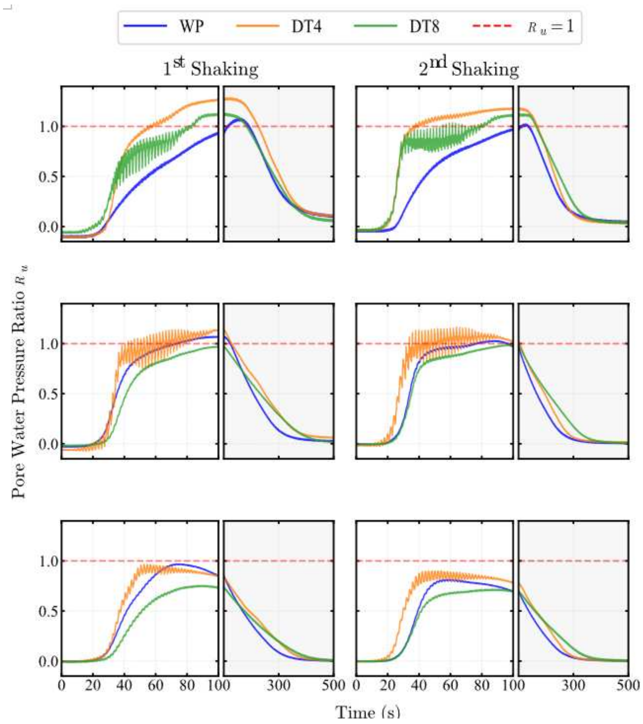

Figure 11. Comparison of EPWP ratio in WP, DT4 and DT8 at first shaking and second shaking

4 CONCLUSION

These results indicate that the initial soil fabric formed by each preparation method affects both the CPT results and the liquefaction resistance under multiple shaking events. In the water pluviation (WP) method, the CPT results showed that the cone tip resistance increased after shaking, suggesting that densification of the soil structure occurred due to cyclic loading. Furthermore, the EPWP ratio results demonstrate that maximum EPWP ratio was lower during the second shaking than during the first, and that the duration for which the EPWP exceeded the initial effective stress was substantially reduced. This behavior is likely because the first shaking caused the soil particles to rearrange into a more stable configuration, thereby enhancing the overall liquefaction resistance of the soil model.

In contrast, both dry tamping (DT) cases exhibited only minor changes in cone tip resistance after shaking and the maximum EPWP ratio during the second shaking remained largely unchanged from the first, and the reduction in liquefaction duration was not as pronounced as in the WP case. Dry-tamped specimens are generally considered to possess an isotropic structure. This isotropy likely limited the extent of structural rearrangement during shaking. Moreover, in the DT4 case, the non-uniformity caused by layer-by-layer compaction was reflected in the CPT results. Consequently, the vertical non-uniformity in the soil model may have facilitated a rapid increase in EPWP, leading to a weaker resistance against shaking.

In conclusion, these findings demonstrate that the sample preparation method plays a crucial role in determining liquefaction resistance and its evolution under repeated shaking events.

REFERENCES

Seed, H.B. (1979). Soil liquefaction and cyclic mobility evaluation for level ground during earthquakes. *Journal of Geotechnical and Geoenvironmental Engineering*, ASCE, 105(GT12), pp. 201–255.

Chen, Y., Yang, J., Chen, Y., and Wei, X. (2025). Variation of elastic shear modulus of sands due to cyclic loadings: the impact of sample preparation methods. *Acta Geotechnica*. http://doi.org/10.1007/s11440-025-02836-z

Carey, T.J., Chiaradonna, A., Love, N.C., Wilson, D.W., Ziotopoulou, K., Martinez, A., and DeJong, J.T. (2022). Effect of soil gradation on embankment response during liquefaction: a centrifuge testing program. *Soil Dynamics and Earthquake Engineering*, 157, 107221. http://doi.org/10.1016/j.soildyn.2022.107221

Florez. (2026). Effect of sand relative density on cone penetration resistance pre- and post-shaking: centrifuge modelling and numerical simulation. Master's Thesis, Graduate School of Engineering, Kyoto University.